AIAA JOURNAL
Vol. 39, No. 9, September 2001

Development of a One-Equation Transition/Turbulence Model

J. R. Edwards*
North Carolina State University, Raleigh, North Carolina 27695
C. J. Roy† and F. G. Blottner‡
Sandia National Laboratories, Albuquerque, New Mexico 87185-0835
and
H. A. Hassan§
North Carolina State University, Raleigh, North Carolina 27695

The development of a unified one-equation model for the prediction of transitional and turbulent flows is described herein. An eddy-viscosity–transport equation for nonturbulent fluctuation growth based on that proposed by Warren and Hassan (Warren, E. S., and Hassan, H. A., "Transition Closure Model for Predicting Transition Onset," *Journal of Aircraft*, Vol. 35, No. 5, 1998, pp. 769–775) is combined with the Spalart–Allmaras one-equation model for turbulent fluctuation growth. Blending of the two equations is accomplished through a multidimensional intermittency function based on the work of Dhawan and Narasimha (Dhawan, S., and Narashima, R., "Some Properties of Boundary Layer Flow During Transition from Laminar to Turbulent Motion," *Journal of Fluid Mechanics,* Vol. 3, No. 4, 1958, pp. 418–436). The model predicts both the onset and extent of transition. Low-speed test cases include transitional flow over a flat plate, a single-element airfoil, a multielement airfoil in landing configuration, and a circular cylinder. Simulations of Mach 3.5 transitional flow over a 5-deg cone are also presented. Results are compared with experimental data, and the spatial accuracy of selected predictions is analyzed.

Nomenclature

a	=	model constant
C_{b1}	=	Spalart–Allmaras[7] model constant
C_t	=	model constant
C_{t3}	=	Spalart–Allmaras[7] model constant
C_{t4}	=	Spalart–Allmaras[7] model constant
C_{w1}	=	Spalart–Allmaras[7] model constant
C_μ	=	model constant
d	=	distance to nearest wall
f_{t2}	=	transition function in Spalart–Allmaras[7] model
f_{v1}	=	wall damping function in Spalart–Allmaras[7] model
f_w	=	wall blockage function in Spalart–Allmaras[7] model
k	=	fluctuation kinetic energy
Re	=	Reynolds number
R_T	=	turbulence Reynolds number
s	=	surface distance
T	=	temperature
Tu	=	turbulence intensity (percentage)
Γ	=	intermittency function
γ	=	ratio of specific heats
δ	=	boundary-layer thickness
ζ	=	enstrophy (vorticity variance)
η	=	localization function
κ	=	von Kármán constant
λ	=	relaxation length
ν	=	kinematic viscosity
ν_{nt}	=	nonturbulent eddy viscosity
$\tilde{\nu}$	=	transported eddy viscosity in Spalart–Allmaras[7] model
ξ	=	variable used in intermittency function
σ	=	model constant
τ	=	timescale
ϕ	=	flow property in Richardson extrapolation
Ω	=	vorticity vector magnitude
ω	=	characteristic frequency of disturbance

Subscripts

aw	=	adiabatic wall
b	=	boundary layer
D	=	diameter
e	=	boundary-layer edge
l	=	laminar
N	=	Narasimha
nt	=	nonturbulent
t	=	transitional or turbulent
w	=	wall
∞	=	freestream conditions
0	=	stagnation conditions

Superscript

$*$	=	boundary-layer reference state

Introduction

EARLIER works[1–5] have detailed the development of a unified modeling approach for transitional/turbulent flows based on the combination of the k–ζ (enstrophy) turbulence model[6] with a model for nonturbulent fluctuation growth.[1,2] Linear stability theory is used to guide the modeling of the nonturbulent fluctuation growth process that leads to transition. Thus far, Tollmien–Schlichting (first-mode), crossflow, bypass, and second-mode mechanisms have been implemented into the k–ζ version, with generally good results having been achieved for a variety of flowfields. The transition model is partially algebraic, in that timescales used to characterize different transition mechanisms depend on some boundary-layer properties, such as edge velocities and boundary-layer displacement thicknesses.

This paper reports on the application of these ideas to one-equation eddy-viscosity–transport turbulence models. Initial

Received 7 August 2000; revision received 22 February 2001; accepted for publication 7 March 2001.

*Associate Professor, Department of Mechanical and Aerospace Engineering, Campus Box 7910; jredward@eos.ncsu.edu. Senior Member AIAA.

†Senior Member of Technical Staff, Thermal/Fluid Computational Engineering Sciences Department, Mail Stop 0835, P.O. Box 5800. Member AIAA.

‡Distinguished Member of Technical Staff, Aerosciences and Compressible Fluid Mechanics Department, Mail Stop 0825, P.O. Box 5800. Fellow AIAA.

§Professor, Department of Mechanical and Aerospace Engineering, Campus Box 7910; hassan@eos.ncsu.edu. Associate Fellow AIAA.

attention is focused on the popular Spalart–Allmaras one-equation model,[7] but the procedures as developed should be applicable to other models of this type. An eddy-viscosity–transport model for nonturbulent fluctuation growth is proposed through analogy with the work of Warren and Hassan.[1,2] Blending of this formulation with the fully turbulent Spalart–Allmaras model[7] is achieved through a multidimensional intermittency function based on the work of Dhawan and Narasimha.[8] The sections that follow present the unified one-equation transition/turbulence model and describe results that illustrate its effectiveness in simulating a variety of transitional flows driven by growth of first-mode disturbances.

Model Description

In the Warren–Hassan transition model,[1,2] the growth of the nonturbulent fluctuation kinetic energy k is modeled by an equation of the following form:

$$\frac{\mathrm{D}k}{\mathrm{D}t} = \nu_{\mathrm{nt}}\Omega\left(\Omega - a\frac{k}{\sqrt{2}\nu}\right) + \frac{\partial}{\partial x_j}\left(\left(\frac{\nu}{3} + 1.8\nu_{\mathrm{nt}}\right)\frac{\partial k}{\partial x_j}\right) \tag{1}$$

where

$$\nu_{\mathrm{nt}} = C_\mu k \tau_{\mathrm{nt}} \tag{2}$$

and Ω is the magnitude of the vorticity vector. The timescale τ_{nt} is characteristic of the prevailing transition mechanism. The present work focuses strictly on transition due to first-mode (Tollmein–Schlicting) disturbances, where

$$\tau_{\mathrm{nt}} = a/\omega_1 \tag{3}$$

In this, ω_1 represents the frequency of the first-mode disturbance having the maximum amplification rate and is correlated as a function of displacement thickness as[1]

$$\omega_1 \nu_e \big/ U_e^2 = 3.2 Re_{\delta^*}^{-\frac{3}{2}} \tag{4}$$

A similar correlation written in terms of the surface distance s is the following[3]:

$$\omega_1 \nu_e \big/ U_e^2 = 0.48 Re_s^{-0.65} \tag{5}$$

This correlation is less suited than Eq. (4) for flows with significant pressure gradient effects, but is less expensive to compute. Of the cases presented later, only the two-dimensional cylinder flows required the use of Eq. (4).

In these descriptions, the subscript e represents an evaluation at the edge of the boundary layer. To account for compressibility effects, the kinematic viscosity ν_e in Eqs. (4) and (5) is evaluated at a reference temperature T^*, defined as[3]

$$T^* \big/ T_e = 1 + 0.032 M_e^2 + 0.56[(T_w/T_e) - 1] \tag{6}$$

The calculation (or estimation) of boundary-layer quantities is a necessary, but somewhat cumbersome aspect of the transition model. In the calculations presented later, the edge conditions were either determined directly through a searching procedure (flat plate, supersonic cone, cylinder flow) or were estimated from the surface pressure distribution by assuming isentropic, adiabatic flow in the inviscid regions and zero pressure gradient in the direction normal to the surface (low-speed airfoils). The quantity s is a surface distance measured from the stagnation point. In the case of transitional flow over a circular cylinder, the displacement thickness required in Eq. (4) was calculated using the Thwaites–Walz integral boundary-layer method, using edge conditions determined from a searching procedure. Other quantities appearing in the formulation include the magnitude of the vorticity vector Ω and the model constant a. The constant a depends on the turbulence intensity; a precise form is presented later.

Equation (1) is converted to an evolution equation for an eddy-viscosity characteristic of nonturbulent fluctuations by multiplying by $C_\mu \tau_{\mathrm{nt}}$ and neglecting derivatives of the surface-dependent quantity τ_{nt}:

$$\frac{\mathrm{D}\nu_{\mathrm{nt}}}{\mathrm{D}t} = \nu_{\mathrm{nt}}\Omega\left(C_\mu \Omega \tau_{\mathrm{nt}} - a\frac{\nu_{\mathrm{nt}}}{\sqrt{2}\nu}\right) + \frac{\partial}{\partial x_j}\left[\left(\frac{\nu}{3} + 1.8\nu_{\mathrm{nt}}\right)\frac{\partial \nu_{\mathrm{nt}}}{\partial x_j}\right] \tag{7}$$

Equation (7) is then combined with the Spalart–Allmaras model,[7] with each component weighted by an intermittency function Γ. As Γ approaches zero, the evolution equation for the non-turbulent eddy viscosity [Eq. (7)] is recovered, and as Γ approaches one, the standard Spalart–Allmaras model is recovered. Using the notation of Ref. 7, the result is given by the following:

$$\begin{aligned}\frac{\mathrm{D}\tilde{\nu}}{\mathrm{D}t} &= (1-\Gamma)\tilde{\nu}\Omega\left[C_\mu \Omega \tau_{\mathrm{nt}} - a\frac{\tilde{\nu}}{\sqrt{2}\nu}\right] + C_t \Gamma(1-\Gamma)\tilde{\nu}\Omega \\ &\quad + \Gamma\left[C_{b1}(1-f_{t2})\tilde{\nu}\tilde{\Omega} - \left(C_{w1}f_w - \frac{C_{b1}}{\kappa^2}f_{t2}\right)\left(\frac{\tilde{\nu}}{d}\right)^2\right] \\ &\quad + \frac{\Gamma}{\sigma}C_{b2}(\nabla\tilde{\nu})^2 + \nabla\cdot\left(\frac{1}{\sigma_l}\nu + \frac{1}{\sigma_t}\tilde{\nu}\right)\nabla\tilde{\nu}\end{aligned} \tag{8}$$

where

$$1/\sigma_l = (\Gamma/\sigma) + [(1-\Gamma)/3] \tag{9}$$

$$1/\sigma_t = (\Gamma/\sigma) + 1.8(1-\Gamma) \tag{10}$$

where $\tilde{\nu}$ is the transported quantity (proportional to the eddy viscosity) and d is the distance from the nearest wall. The term $C_t\Gamma(1-\Gamma)\tilde{\nu}\Omega$, which is not present in either Eq. (7) or the Spalart–Allmaras model, affects the behavior of the solution in the transition region $0 < \Gamma < 1$. The chosen value of C_t, 0.35, was determined by numerical optimization, as discussed later. The final step accounts for the viscous sublayer in the fully turbulent region:

$$\nu_t = \tilde{\nu}[1 + \Gamma(f_{v1} - 1)] \tag{11}$$

This step turns off viscous damping in the regions governed by nonturbulent fluctuations. All other constants and functions are as described in Ref. 7, except that the function

$$f_{t2} = C_{t3}\exp\left[-C_{t4}(\tilde{\nu}/\nu)^2\right] \tag{12}$$

is redefined as

$$f_{t2} = C_{t3}\exp\left(-C_{t4}\left\{\max\left[\frac{\sqrt{2}C_\mu\Omega\tau_{\mathrm{nt}}}{(a+b)}, \frac{\tilde{\nu}}{\nu}\right]\right\}^2\right) \tag{13}$$

The additional argument in Eq. (13) the algebraic solution of Eq. (7), neglecting convective and diffusive terms. This modification helps initiate the turbulent growth process. The trip term described in Ref. 7 is not included.

Transition Onset

Transition onset is specified by monitoring the behavior of the quantity

$$R_T = \tilde{\nu}/C_\mu\nu \tag{14}$$

throughout a particular boundary-layer profile. When the maximum value of R_T in a profile first exceeds unity (first in the sense of a sweep from the stagnation point aft), transition onset is assumed to occur, and the surface distance from that point to the stagnation point is designated as s_t. This step is one of the more geometry-dependent aspects of the model but is somewhat better than other onset indicators, such as the point of minimum heat flux or skin friction, for complex configurations. In Ref. 1 it is shown that, for simpler flowfields, the R_T criterion gives results nearly equivalent to those obtained using a minimum skin-friction indicator of transition onset.

Intermittency Definition

The nonturbulent and turbulent components of Eq. (9) are blended through the intermittency function Γ. This is composed of two parts, a surface-distance-dependent component $\Gamma_N(s)$ based on the work of Dhawan and Narasimha[8] and a multidimensional component $\Gamma_b(x, y)$ that serves to restrict the applicable range of the transition model to boundary layers. The particular form is given as follows:

$$\Gamma(x, y) = 1 + \Gamma_b(x, y)[\Gamma_N(s) - 1] \tag{15}$$

The Dhawan–Narasimha expression Γ_N is defined along the surface of the geometry from the stagnation point:

$$\Gamma_N(s) = 1 - \exp(-0.412\xi^2) \tag{16}$$

$$\xi = \max(s - s_t, 0)/\lambda \tag{17}$$

$$Re_\lambda = 9.0 Re_{s_t}^{-0.75} \tag{18}$$

The boundary-layer localization function Γ_b is defined as follows:

$$\Gamma_b(x, y) = \tanh(\eta^2) \tag{19}$$

$$\eta = \frac{\max[0, \max(t_1, t_2) - t_\infty]}{t_3 + t_\infty} \tag{20}$$

$$t_1 = \frac{500\nu}{d^2} \tag{21}$$

$$t_2 = \frac{\sqrt{(\nu + \nu_t)\Omega}}{C_\mu^{\frac{3}{2}} d} \tag{22}$$

$$t_3 = \sqrt{C_\mu}\Omega \tag{23}$$

$$t_\infty \approx 1 \times 10^{-7} \frac{U_\infty^2}{\nu_\infty} \tag{24}$$

This expression is similar to that utilized in Menter's hybrid k–ϵ/k–ω turbulence model.[9] Γ_b approaches one near solid surfaces and decays sharply to zero as the edge of the boundary layer is approached. For simpler flows, one can also use

$$\Gamma(x, y) = \Gamma_N(s) \tag{25}$$

with equivalent results. The utility of the multidimensional component Γ_b lies in the calculation of transitional flows on complex geometries, where both shear layers (treated as fully turbulent) and boundary layers might be present.

Results

The unified transition/turbulence model described in earlier sections has been implemented into two Navier–Stokes codes: a research version of CFL3D,[10] a cell-centered finite volume Navier–Stokes solver for three-dimensional aerodynamic flows, and REACTMB,[11] a cell-vertex finite volume Navier–Stokes solver for two-dimensional or axisymmetric reactive flows. The research version of CFL3D[12] utilizes time-derivative preconditioning[13] to enhance solution accuracy and numerical efficiency for low-speed flow calculations. REACTMB also utilizes time-derivative preconditioning. In CFL3D, the unified model is advanced in a weakly coupled manner, with the solution for eddy viscosity updated after the solution for the main flow variables. In REACTMB, the model is strongly coupled with the main flow equations. A baseline convergence criterion of a seven-decade reduction in the residual norm was used for REACTMB, with the cases used in the grid convergence studies converged to even tighter tolerances. Convergence for CFL3D was assessed by monitoring lift and drag coefficients and predicted transition points because residual norms tended to oscillate after a period of rapid decrease.

Validation of the new approach is accomplished through simulations of five low- and high-speed flows, four of which were successfully computed by the original Warren–Hassan[1,2] transition/turbulence model. Simulations of the flat-plate experiments of Schubauer and Klebanoff,[14] and Schubauer and Skramstad[15] are used to determine the functional dependence of the model constant a on the freestream turbulence intensity Tu, expressed as a percentage value. The results, obtained by correlating the predicted transition onset locations with experimental data, yield the following dependence:

$$a = 0.009863 - 0.001801(Tu) + 0.05050(Tu)^2 \tag{26}$$

Note that the calibration is also sensitive to the freestream value of the transported quantity $\tilde{\nu}$. This is chosen as $0.0001\nu_\infty$ for all calculations presented herein. The effect of the constant C_t in Eq. (9) on the skin-friction predictions for the Schubauer–Klebanoff[14] experiment ($Tu = 0.03$) is shown in Fig. 1 (CFL3D implementation). All choices predict the correct onset location based on the $R_T = 1$ criterion, as per the calibration, but the shape of the skin-friction distribution is best predicted by the optimized value of $C_t = 0.35$. This value is maintained for all subsequent calculations.

In addition to the 65×97 grid, medium (129×193) and fine (257×385) mesh levels are used to assess the accuracy of the CFL3D solutions. In addition, the Richardson extrapolation procedure (see Ref. 16) is used to obtain more accurate skin-friction profiles:

$$\phi_{\mathrm{RE}} = \phi_1 + (\phi_1 - \phi_2)/3 \tag{27}$$

where 1 and 2 denote the fine- and medium-grid solutions, respectively, and ϕ is the skin friction. Richardson extrapolation assumes that the spatial accuracy is second order and that the solutions are in the asymptotic grid convergence regime. Figure 2 presents computed

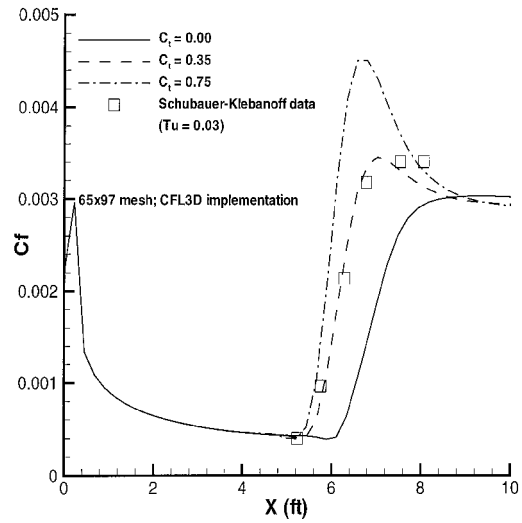

Fig. 1 Effect of C_t on skin-friction distribution: Schubauer–Klebanoff[14] experiment, 65×97 mesh, CFL3D implementation.

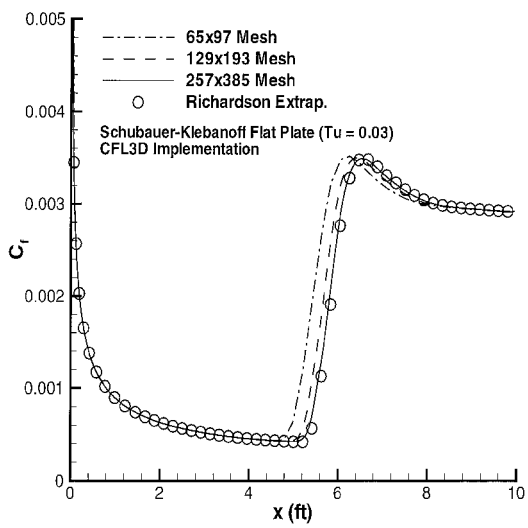

Fig. 2 Skin-friction distributions for the Schubauer–Klebanoff[14] flat plate along with Richardson extrapolation results: CFL3D implementation.

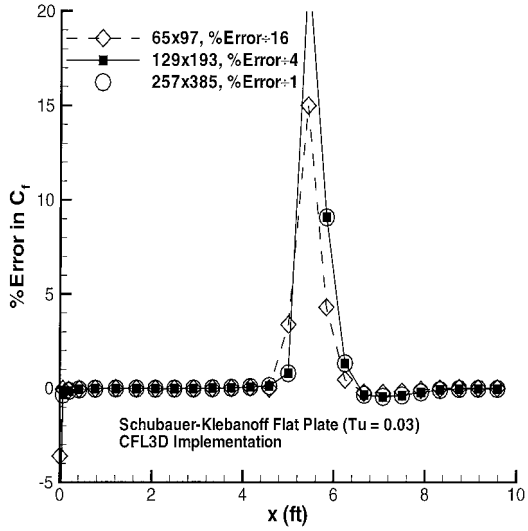

Fig. 3 Normalized error in skin friction on the three mesh levels for the Schubauer–Klebanoff[14] flat plate: CFL3D implementation.

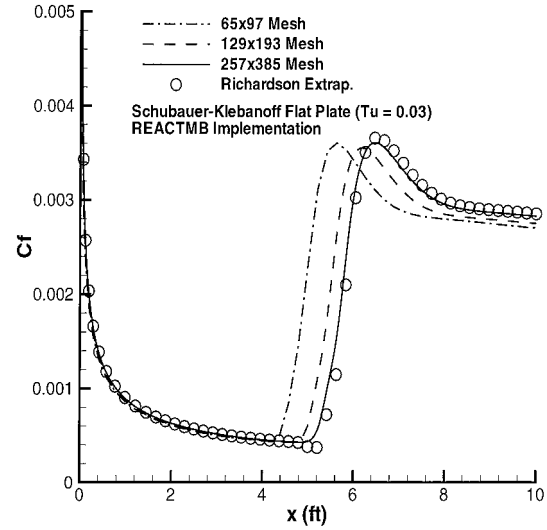

Fig. 4 Skin-friction distributions for the Schubauer–Klebanoff[14] flat plate along with Richardson extrapolation results: REACTMB implementation.

skin-friction profiles for the three grid levels along with the Richardson extrapolation results. Only the results in the transitional region appear to show dependence on the mesh size. The assumptions that the solutions are second-order accurate and in the asymptotic grid convergence regime can be assessed by examining the percent error in the solution values relative to the Richardson extrapolation value:

$$\%\ \text{error of mesh}\, k = [(\phi_k - \phi_{\text{RE}})/\phi_{\text{RE}}] \times 100 \tag{28}$$

For these assumptions to hold, it is necessary (although not sufficient) that the percent error obey the relationship

$$\%\ \text{error of mesh 1} = (\%\ \text{error of mesh 2})/4$$

$$= (\%\ \text{error of mesh 3})/16 \tag{29}$$

where the left equality in Eq. (29) is identically true when Eq. (27) is used. The normalized errors from Eq. (28) are presented in Fig. 3 for the CFL3D solutions of the Schubauer–Klebanoff[14] flat plate case. The skin friction in the laminar and turbulent regions does appear to be within the second-order asymptotic grid convergence regime. The fine-grid errors in this region are below 1%, whereas the solutions in the transitional region do not appear to be fully grid converged. This latter result is not surprising because no attempt has been made to provide a priori clustering in this region.

Figure 4 shows the effect of grid refinement on the skin-friction prediction for the $Tu = 0.03$ case, REACTMB implementation. Again, solutions are presented on the three mesh levels along with the Richardson extrapolation results. Grid sensitivity is seen in both the transitional and turbulent regions of the flow. Figure 4 also shows that the predicted transition location and the extent of the transition region display some sensitivity to the mesh size. The normalized errors from Eq. (29) are presented in Fig. 5 and show that the fine-grid solution is accurate to within 1% in the laminar region and approximately 3% in the turbulent region. Although these errors are small, the fact that the normalized errors do not satisfy Eq. (29) indicates that the assumptions required for the application of Richardson extrapolation are not fully valid. Thus, the error estimates presented in Fig. 5 may not be accurate. It is expected that these errors could be further reduced with additional grid refinement and/or grid adaptation. Finally, Fig. 6 compares fine-grid solutions from the two codes with experimental data for the $Tu = 0.03$ case. Even with significant grid refinement, the solutions do display some code- and implementation-dependent differences.

The second case considered involves the database of Mateer et al.,[17] which contains skin-friction measurements over a supercritical airfoil for a freestream Mach number of 0.2 and a range of Reynolds numbers and angles of attack. The percentage turbulence intensity is $Tu = 0.5$, higher than the highest value found in the Schubauer–Skramstad[15] database ($Tu = 0.34$). For this level of intensity, the model operates slightly outside its limits of calibration.

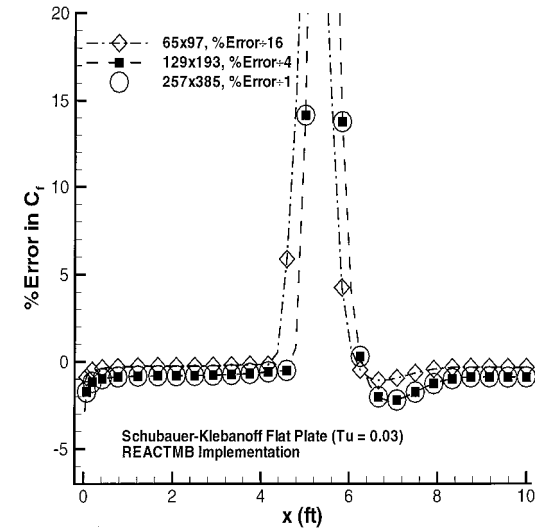

Fig. 5 Normalized error in skin friction on the three mesh levels for the Schubauer–Klebanoff[14] flat plate: REACTMB implementation.

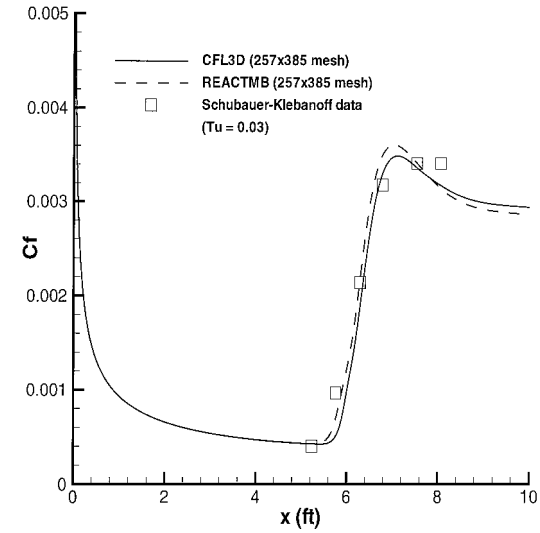

Fig. 6 Fine-grid skin-friction predictions vs experimental data: Schubauer–Klebanoff[14] experiment.

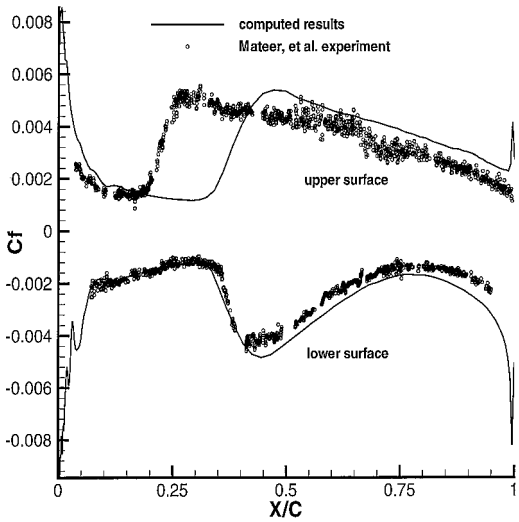

Fig. 7 Skin-friction distributions: Mateer et al.[17] supercritical airfoil, $Re_c = 2 \times 10^6$, 321×91 mesh.

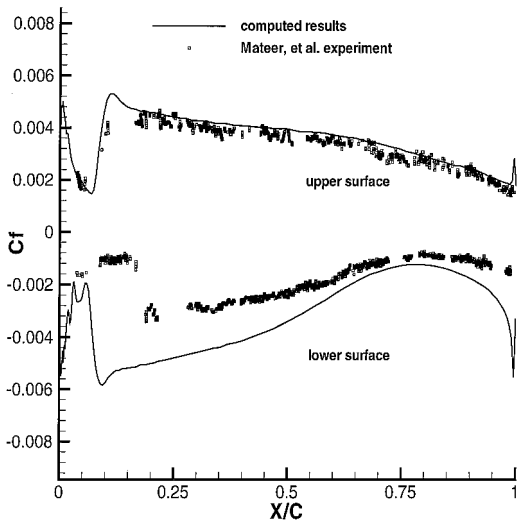

Fig. 8 Skin-friction distributions: Mateer et al.[17] supercritical airfoil, $Re_c = 6 \times 10^6$, 321×91 mesh.

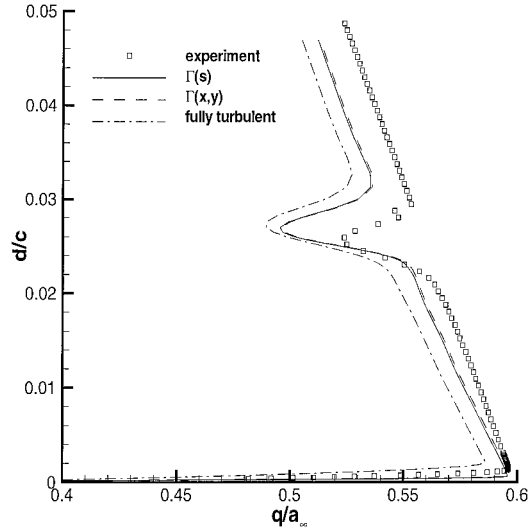

Fig. 9 Velocity profiles: $x/c = 0.1075$ station and $\alpha = 19$ deg.

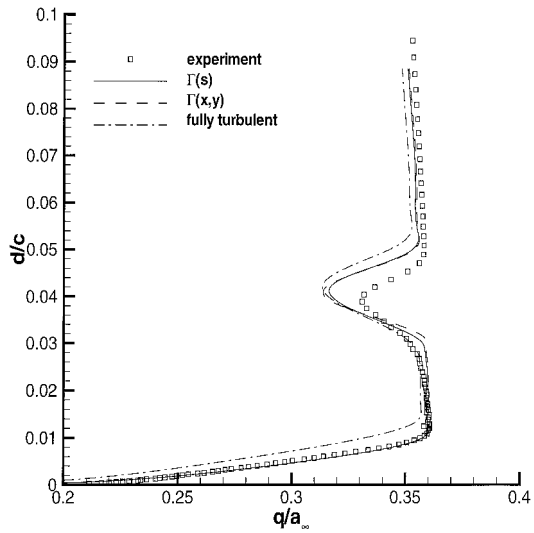

Fig. 10 Velocity profiles: $x/c = 0.45$ station and $\alpha = 19$ deg.

Figure 7 presents skin-friction distributions for a Reynolds number of 2×10^6 (based on a 0.2-m chord) and an angle of attack of −0.5 deg. The CFL3D implementation is used for this case. Calculations from a boundary-layer integral/e^n analysis yielded transition predictions well aft of the experimental results for both surfaces.[17] The unified one-equation model predicts transition accurately on the lower surface but aft of the experimental location on the upper surface. These results are in accord with those presented earlier for the Warren–Hassan implementation.[1] Figure 8 compares predictions and experimental results for a higher Reynolds number of 6×10^6. Good agreement with the upper-surface transition location is indicated, but the model underpredicts the extent of laminar flow on the lower surface. Note that the predicted transition locations for both cases are nearly equal for the upper and lower surfaces, a trait also shared by the Warren–Hassan implementation. This may indicate the need for the explicit inclusion of surface pressure gradient effects into the correlation for τ_{nt} to render it more valid for curved surfaces.

The third test case involves Mach 0.2, $\alpha = 19$ deg flow about a three-element airfoil in landing configuration.[18–20] This configuration has been the subject of a detailed investigation using the original Warren–Hassan[1,2] transition/turbulence model.[4] Results using the baseline Spalart–Allmaras[7] model with either user-specified transition points or natural transition have also been reported.[19] Figures 9, 10, and 11 compare velocity magnitude profiles at the $x/c = 0.1075$, $x/c = 0.45$, and $x/c = 0.8982$ locations (relative to the stowed chord length) with experimental data from Chin et al.[18] Profiles were measured only along the upper surfaces of the airfoils and are plotted vs normal distance from the surface. These calculations were run using the modified CFL3D code, assuming a freestream turbulence intensity of $Tu = 0.05$. Figures 9–11 include results from the unified model implemented using the one-dimensional intermittency function $\Gamma = \Gamma_N(s)$ [Eq. (25)], results from the unified model implemented using the two-dimensional intermittency function $\Gamma = \Gamma(x, y)$ [Eq. (15)], and results from a fully turbulent implementation. In comparison with the fully turbulent model, the unified model provides better agreement with experimental data for the stations on the main element but provides poorer agreement on the flap. Close agreement between predictions using the one-dimensional intermittency function and those using the two-dimensional intermittency function is evidenced for all stations. The success of the one-dimensional intermittency function in this case may be fortuitous, because the grid blocking arrangement is such that the presence of transitional regions extending away from the element surfaces does not interfere significantly with turbulent wake development. In accord with experimental results,[20] the unified model predicts a nearly laminar slat cove and a nearly laminar undersurface of the flap. The model does, however, predict transition on the lower surface of the main element as occurring at roughly the quarter-chord point. Experimental data suggest that transition on this surface is delayed until the flap cove.

The fourth test case involves Mach 0.07 flow over a heated circular cylinder of diameter 0.1472 m and corresponds to experiments conducted by Achenbach.[21] The database of Achenbach provides

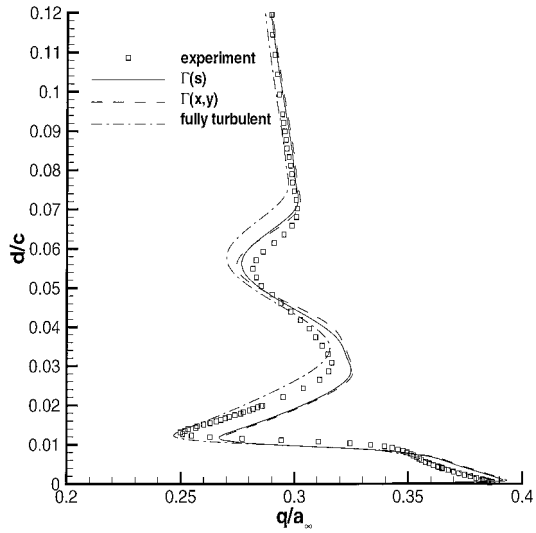

Fig. 11 Velocity profiles: $x/c = 0.8982$ station and $\alpha = 19$ deg.

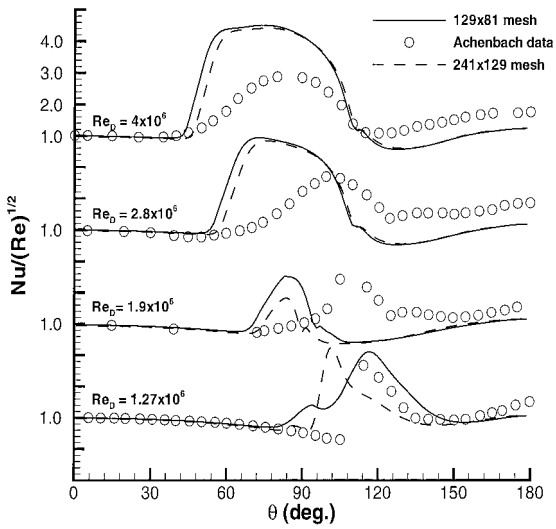

Fig. 12 Nusselt number vs circumferential angle: Achenbach[21] experiment.

surface heat transfer, wall shear, and surface pressure measurements for Reynolds numbers ranging from subcritical values ($Re_D = 10^5$) to supercritical values ($Re_D = 4 \times 10^6$). The level of accuracy of the data is uncertain, but it appears to be the only database that provides heat transfer and shear stress measurements over a wide range of conditions. The simulations assume that the effects of all modes of time-dependent behavior, including vortex shedding, are accounted for by the turbulence model; thus, the calculations attempt to attain the long-time averaged solution. Centerline symmetry is enforced, and the calculations are performed on 129×81 and 241×129 O-type meshes, clustered to the cylinder surface. Part of the outer boundary of the grid is chosen to conform to the outer tunnel wall, and a slip wall boundary condition is imposed over this portion to account for possible wall blockage effects. A freestream temperature of 303 K is assumed, and the wall temperature is set to 1.066 times the freestream value. As mentioned in the "Model Description" section, τ_{nt} is based on the boundary-layer displacement thickness, which is calculated from an integral boundary-layer method. A percentage turbulence intensity of $Tu = 0.45$ is assumed, as per the experiment.

Figures 12 and 13 present Nusselt number and skin-friction distributions vs circumferential angle θ, measured from the forward stagnation point. Nusselt number distributions are presented for supercritical Reynolds numbers of $Re_D = 1.27 \times 10^6$, 1.9×10^6, 2.8×10^6, and 4×10^6, whereas wall shear distributions are presented only for $Re_D = 1.27 \times 10^6$ and 4×10^6. All of the simulated

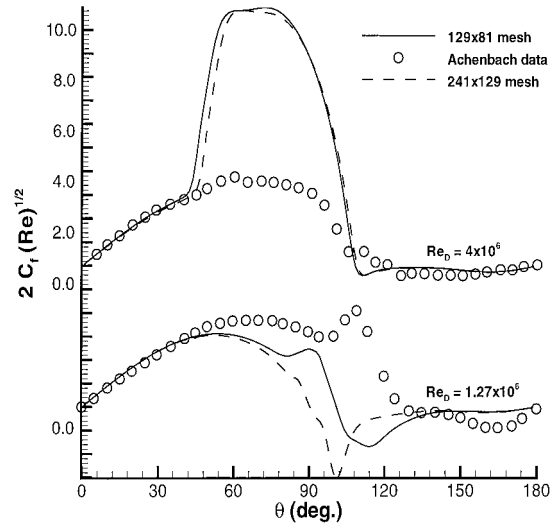

Fig. 13 Skin friction vs circumferential angle: Achenbach[21] experiment.

cases involve transition in the boundary layer before its separation from the cylinder surface. As of now, the model does not include any provision for separation-induced transition or transition in a wake; thus, critical and subcritical Reynolds number cases were not attempted.

Figures 12 and 13 indicate that the present model predicts the onset of transition reasonably well, with minor differences observed in the onset location with mesh refinement. As the Reynolds number decreases, the transition point moves farther away from the forward stagnation point. For the highest three Reynolds numbers, steady solutions were obtained. At the lowest Reynolds number of 1.27×10^6, transition onset is predicted to occur very near the point of initial flow separation (Fig. 13). Because the transition length provided by the intermittency function Γ increases as the distance to the onset location increases, the model does not produce enough eddy viscosity to allow steady solutions to be obtained for this case. The results presented were averaged over 30 characteristic times, and the coarse-mesh distributions in particular indicate the effects of time-dependent shifting of the onset location.

The extent of transition and the peak values of heat transfer and skin-friction coefficient are not well predicted. The experimental data indicate a much more intermittent response than the current Dhawan–Narasimha[8] formulation will produce. Other researchers[22,23] have reported similar levels of disagreement with Achenbach's[21] skin-friction data. Some improvement might be gained by including pressure gradient effects explicitly into the intermittency formulation. However, most of the proposed modifications of this type only affect favorable pressure gradient flows minimally. A better alternative might be to relax the centerline symmetry assumption and run the simulation as a completely unsteady flow, following Ref. 23, to determine whether a very large-scale, time-dependent movement of the onset location might be captured.

The last test case considered involves transitional, Mach 3.5 flow over a 5-deg half-angle cone and corresponds to a set of experiments conducted by Chen et al.[24] in the NASA Langley Research Center Mach 3.5 Pilot Low Disturbance Wind Tunnel. This case has also been studied by Singer et al.,[25] Warren et al.,[26] and McDaniel et al.,[3] with the two latter efforts using variants of the Warren–Hassan[1,2] transition model. Figure 14 presents wall recovery factor as a function of surface distance along the cone. The wall recovery factor is defined by the relation

$$r = (T_{aw} - T_e)/(T_0 - T_e)$$

where

$$T_0 = T_e\left\{1 + [(\gamma - 1)/2]M_e^2\right\}$$

and T_{aw} and T_e are determined from the computed solution at the wall and at the edge of the boundary layer. The calculations assume

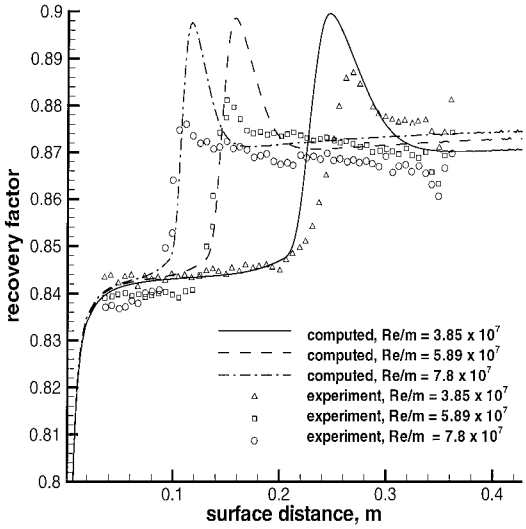

Fig. 14 Measured and computed recovery factors: $M = 2.5$ and $Pr_t = 0.88$.

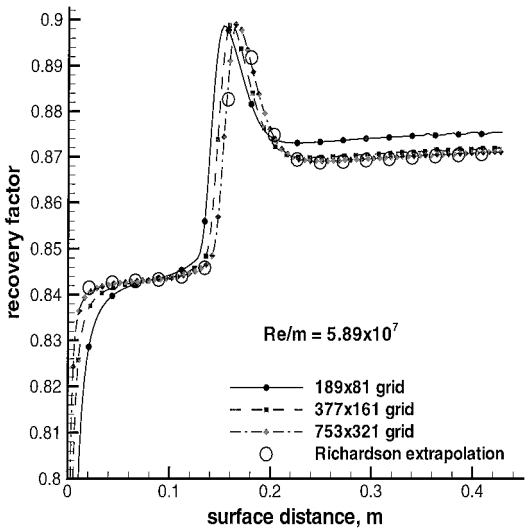

Fig. 15 Recovery factor distributions for the Mach 3.5 cone along with Richardson extrapolation results.

that only first-mode mechanisms are important and assume a turbulent Prandtl number of 0.88 and a turbulence intensity of 0.05. Furthermore, the calculations were performed using the REACTMB implementation. As noted in Ref. 26, recovery factor predictions for this flow are very sensitive to the assumed value of the turbulent Prandtl number, with the commonly used value of 0.9 resulting in a sizeable overprediction in the transitional and turbulent regions. In Ref. 26, it is also shown that agreement with experimental data can be substantially improved by including a flow-dependent turbulent Prandtl number; such techniques have yet to be implemented in the present work. The current results indicate that the unified one-equation model accurately predicts the onset of transition for each of the Reynolds numbers considered. The model does overestimate the peak in recovery factor near the end of the transition region and slightly overpredicts the recovery factor in the fully turbulent region. The former effect may indicate the need for improved modeling of the transition-region term

$$C_t \Gamma(1 - \Gamma)\tilde{\nu}\Omega$$

in Eq. (9) for high-speed flows.

Three grid levels are used to assess the accuracy of the calculations for the $Re/m = 5.89 \times 10^7$ case. Figure 15 shows the recovery factor profiles for the three grid levels along with the Richardson extrapolation results using Eq. (27). The most noteworthy effects of increasing mesh refinement are a decrease in the distance required

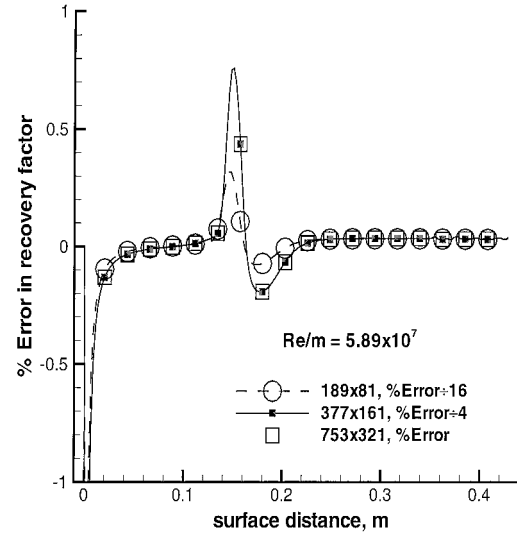

Fig. 16 Normalized error in recovery factor on the three mesh levels for the Mach 3.5 cone.

to establish an equilibrium laminar boundary layer, a lowering of the recovery factor in the fully turbulent region, and a slight shift in the transition onset location downstream. The errors in recovery factor relative to the more accurate extrapolated values are given in Fig. 16, where the errors have been normalized according to Eq. (29). The fine-grid errors are well below 0.1% in the laminar and turbulent regions. The collocation of the normalized errors indicates the locations where the solution is likely in the asymptotic grid convergence regime. Larger errors are seen at the stagnation point singularity and in the transition region due to the large gradients. Additional grid clustering could be employed to reduce the magnitude of the error in these regions.

Conclusions

A unified, one-equation eddy-viscosity–transport model for transitional and turbulent flows has been developed. The model combines an evolution equation for nonturbulent fluctuation growth developed from the work of Warren and Hassan[1,2] with the standard Spalart–Allmaras[7] turbulence model. Blending of the two equations is accomplished through a multidimensional intermittency function. The current formulation is calibrated for transition driven by the growth of first-mode instabilities and predicts both the onset and extent of the transition region. The model has been applied with reasonable success to transitional flows over a flat plate, a supercritical airfoil, a multielement airfoil in landing configuration, a circular cylinder, and a sharp cone. The predictions are very similar to those obtained earlier using the k–ζ turbulence model, indicating that the performance of the Warren–Hassan[1,2] model in predicting transitional flows is relatively independent of the turbulence model used. Grid refinement studies for selected cases indicate that the prediction of transition onset is relatively insensitive to the grid spacing for the finer meshes but that grid refinement or grid adaptation may be required to obtain grid independence in the prediction of the extent of the transition region. Work is in progress to include other transition mechanisms into the model and to incorporate pressure gradient effects explicitly into the formulation. Further work will be required to extend the approach toward three-dimensional flows. In particular, alternatives to the use of geometry-dependent, boundary-layer-type quantities should be devised, and methods for accounting for the effects of multiple transition modes must be developed.

Acknowledgments

This research is sponsored by Sandia National Laboratories, a multiprogram laboratory operated by Sandia Corporation, a Lockheed Martin Company, for the U.S. Department of Energy under Contract DE-AC04-94AL85000, under Contract BF-856. Cray T-90 computer time is provided by a grant from the North Carolina Supercomputing Center.

References

[1]Warren, E. S., and Hassan, H. A., "Transition Closure Model for Predicting Transition Onset," *Journal of Aircraft*, Vol. 35, No. 5, 1998, pp. 769–775.

[2]Warren, E. S., and Hassan, H. A., "An Alternative to the e^n Method for Determining Onset of Transition," AIAA Paper 97-0825, Jan. 1997.

[3]McDaniel, R. D., Nance, R. P., and Hassan, H. A., "Transition Onset Prediction for High Speed Flow," AIAA Paper 99-3792, June 1999.

[4]Czerwiec, R., Edwards, J. R., Rumsey, C. L., Bertelrud, A., and Hassan, H. A., "Study of High-Lift Configurations Using k–ζ Transition/Turbulence Model," *Journal of Aircraft*, Vol. 37, No. 6, 2000, pp. 1008–1016.

[5]McDaniel, R. D., and Hassan, H. A., "Study of Bypass Transition Using the k–ζ Framework," AIAA Paper 2000-2310, June 2000.

[6]Robinson, D. F., and Hassan, H. A., "Further Development of the k–ζ (Enstrophy) Turbulence Closure Model," *AIAA Journal,* Vol. 36, No. 10, 1998, pp. 1825–1833.

[7]Spalart, P. R., and Allmaras, S. R., "A One-Equation Turbulence Model for Aerodynamic Flows," *La Recherche Aerospatiale*, Vol 1, 1994, pp. 5–21.

[8]Dhawan, S., and Narasimha, R., "Some Properties of Boundary Layer Flow During Transition from Laminar to Turbulent Motion," *Journal of Fluid Mechanics,* Vol. 3, No. 4, 1958, pp. 418–436.

[9]Menter, F. R., "Two-Equation Eddy Viscosity Turbulence Models for Engineering Applications," *AIAA Journal*, Vol. 32, No. 8, 1994, pp. 1598–1605.

[10]Thomas, J. L., Taylor, S. L., and Anderson, W. K., "Navier–Stokes Computations of Vortical Flows over Low Aspect Ratio Wings," AIAA Paper 87-0207, 1987.

[11]McDaniel, K. S., and Edwards, J. R., "Simulation of Thermal Choking in a Model Scramjet Combustor," AIAA Paper 99-3411, June 1999.

[12]Edwards, J. R., and Thomas, J. L., "Development of $\mathcal{O}(Nm^2)$ Preconditioned Multigrid Solvers for the Euler and Navier–Stokes Equations," *AIAA Journal*, Vol. 38, No. 4, 2000, pp. 717–720.

[13]Weiss, J. M., and Smith, W. A., "Preconditioning Applied to Variable and Constant Density Time-Accurate Flows on Unstructured Meshes," AIAA Paper 94-2209, June 1994.

[14]Schubauer, G. B., and Klebanoff, P. S., "Contributions on the Mechanism of Boundary Layer Transition," NACA Rept. 1289, 1956.

[15]Schubauer, G. B., and Skramstad, H. K., "Laminar Boundary Layer Oscillation on a Flat Plate," NACA Rept. 909, 1948.

[16]Roache, P. J., "Systematic Grid Convergence Studies and the Grid Convergence Index (GCI)," *Verification and Validation in Computational Science and Engineering*, Hermosa, Albuquerque, NM, 1998, Chap. 5, p. 109.

[17]Mateer, G. G., Monson, D. J., and Menter, F. R., "Skin-Friction Measurements and Calculations on a Lifting Airfoil," *AIAA Journal*, Vol. 34, No. 2, 1996, pp. 231–236.

[18]Chin, V. D., Peters, D. W., Spaid, F. W., and McGhee, R. J., "Flowfield Measurements About a Multi-Element Airfoil at High Reynolds Numbers," AIAA Paper 93-3137, July 1993.

[19]Rumsey, C. L., Gatski, T. B., Ying, S. Y., and Bertelrud, A., "Prediction of High-Lift Flows Using Turbulent Closure Models," *AIAA Journal*, Vol. 36, No. 5, 1998, pp. 765–774.

[20]Bertelrud, A., "Transition on a Three-Element High-Lift Configuration at High Reynolds Numbers," AIAA Paper 98-0703, Jan. 1998.

[21]Achenbach, E., "Total and Local Heat Transfer From a Smooth Circular Cylinder in Cross-Flow at High Reynolds Number," *International Journal of Heat and Mass Transfer*, Vol. 18, No. 12, 1975, pp. 1387–1396.

[22]Celik, I., and Shaffer, F. D., "Long Time-Averaged Solutions of Turbulent Flow Past a Circular Cylinder," *Journal of Wind Engineering and Industrial Aerodynamics*, Vol. 56, No. 2–3, 1995, pp. 185–212.

[23]Travin, A., Shur, M., Strelets, M., and Spalart, P., "Detached-Eddy Simulations Past a Circular Cylinder," *Flow, Turbulence, and Combustion*, Vol. 63, No. 1–4, 1999, pp. 293–313.

[24]Chen, F. J., Malik, M. R., and Beckwith, I. E., "Boundary-Layer Transition on a Cone and Flat Plate at Mach 3.5," *AIAA Journal*, Vol. 27, No. 6, 1989, pp. 687–693.

[25]Singer, B. A., Dinavahi, S. P. G., and Iyer, V., "Testing of Transition Region Models: Test Cases and Data," NASA CR 4371, May 1991.

[26]Warren, E. S., Harris, J. E., and Hassan, H. A., "Transition Model for High-Speed Flow," *AIAA Journal*, Vol. 33, No. 8, 1995, pp. 1391–1397.

R. M. C. So
Associate Editor